# Reactivity of Carbon Nanofibers with Fluorine Gas

F. Chamssedine,[†] M. Dubois,[†] K. Guérin,[†] J. Giraudet,[‡] F. Masin,[‡] D. A. Ivanov,[⊥] L. Vidal,[⊥] R. Yazami,[§] and A. Hamwi*,[†]

*Laboratoire des Matériaux Inorganiques, UMR CNRS 6002-Université Blaise Pascal, 24 avenue des Landais, 63177 Aubière Cedex, France, Matière Condensée et Résonance Magnétique, Université Libre de Bruxelles, CP 232, Boulevard du Triomphe, B-1050 Bruxelles, Belgium, CALTECH-CNRS, International Laboratory on Materials for Electrochemical Energetics, Pasadena, California 91125, and Institut de chimie des surfaces et interfaces de Mulhouse, UPR CNRS 9069, 15 rue Jean Starcky, 68057 Mulhouse Cedex, France*

*Received July 25, 2006. Revised Manuscript Received October 6, 2006*

The present study highlights the reactivity of carbon nanofibers (CNFs) with fluorine gas. Highly purified and graphitized CNFs were treated under a stream of fluorine gas for 16 h at temperatures ranging from 380 to 480 °C. Different fluorination temperature zones have been revealed by direct physicochemical analysis such as XRD, Raman spectroscopy, EPR, and solid-state NMR ($^{13}C$ and $^{19}F$). The comparison between various parameters such as covalence of C−F bond, $T_1$ spin−lattice nuclear relaxation time, density, and environment of the dangling bonds, among others, allows the fluorination mechanism to be determined, i.e., the formation of $(C_2F)_n$ type graphite fluoride as the precursor of richer $(CF)_n$ compound. This is supported by TEM characterization as the fluorination proceeds from the external parts of the carbon nanofibers and then propagates through the core without a major structural change of the fluorinated parts. A low exfoliation of the sheets is necessary for extended fluorination and conversion into $(CF)_n$; this occurs for fluorination temperatures higher than 472 °C, with concomitant disappearance of the graphitic structure.

## Introduction

The reactivity of carbon allotropic forms with fluorine gas differs largely because of either the degree of graphitization or the type of the carbon material.[1] The higher the degree of graphitization or the number of shells, the higher the temperature required for fluorination. Because of their many industrial applications, such as electrode material for primary lithium batteries,[2,3] solid lubricants,[4,5] or as reservoir for very active molecular oxidizers such as $BrF_3$ and $ClF_3$,[6] these material have been extensively studied.

When graphite is used as the starting material, no significant fluorination is observed below 300 °C. From 350 to 640 °C,[7] two graphite fluorides, mainly differing in crystal structure and composition, are formed: poly(dicarbon monofluoride) $(C_2F)_n$ and poly(carbon monofluoride) $(CF)_n$.[8] In both compounds, the carbon atoms take the $sp^3$ hybridization with associated distortion of the carbon hexagons from planar to chairlike or boatlike configuration. Poly(dicarbon monofluoride) is obtained at ∼350 °C and has a characteristic structure in which two adjacent fluorine layers are separated by two carbon layers bonded by strongly covalent C−C bonding along the *c*-axis of the hexagonal lattice. On the other hand, poly(carbon monofluoride), which is achieved at ∼600 °C, has a structure with only one carbon layer between two adjacent fluorine layers (stage 1). Graphite fluorides obtained between 350 and 600 °C have intermediary composition between $(C_2F)_n$ and $(CF)_n$ and consist of a mixture of these two phases.[8]

Only a few works have been devoted to the fluorination of carbon nanofibers, concerning fluorine−graphite fiber intercalation compounds[9] and fluorinated carbon nanotubes and nanofibers.[10]

Carbon nanotubes have been synthesized in different forms as single-, double- and multiwalled carbon nanotubes, denoted as SWCNT, DWCNT, and MWCNT, respectively. The diameter size ranges between about 2 nm in SWCNTs and DWCNTs to about 20 nm in MWCNTs and to greater than 150 nm in other CNTs or carbon nanofibers (CNFs).

The fluorination temperature of MWCNTs is significantly increased in comparison with SWCNT because of the presence of graphitic multilayers surrounding the nanotube core. This temperature depends on the number of MWCNT

* Corresponding author. Tel: 33 4 73 40 71 03. Fax: 33 4 73 40 71 08. E-mail: andre.hamwi@univ-bpclermont.fr.
[†] Université Blaise Pascal.
[‡] Université Libre de Bruxelles.
[§] CALTECH-CNRS.
[⊥] Institut de chimie des surfaces et interfaces de Mulhouse.

(1) Hamwi, A.; *J. Phys. Chem. Solids* **1996**, *57* (6−8), 677−688.
(2) Watanabe, N.; Nakajima, T.; Touhara, H. *Graphite Fluorides*; Elsevier: Amsterdam, 1988.
(3) Hagiwara, R.; Lerner, M.; Bartlett, N.; Nakajima, T. *J. Electrochem. Soc.* **1988**, *135* (9), 2393.
(4) Fusaro, R. L.; Sliney, H. E. *ASLE Trans.* **1970**, *1* (1), 56.
(5) Fusaro, R. L. *Wear* **1979**, *53* (2), 303.
(6) Nazarov, A. S.; Makotchenko, V. G. *Inorg. Mater.* **2002**, *38* (3), 278.
(7) Nakajima, T.; Watanabe, N. *Graphite Fluorides and Carbon−Fluorine Compounds*; CRC Press: Boston, 1991.
(8) Kita, Y.; Watanabe, N.; Fujii, Y. *J. Am. Chem. Soc.* **1979**, *101*, 3832.
(9) Nakajima, T.; Watanabe, N.; Kameda, I.; Endo, M. *Carbon* **1986**, *24* (3), 343.
(10) Hayashi, T.; Terrones, M.; Scheu, C.; Kim, Y. A.; Ruehle, M.; Nakajima, T.; Endo, M. *Nano Lett.* **2002**, *2* (5), 491.

10.1021/cm061731m CCC: $37.00 © 2007 American Chemical Society
Published on Web 12/23/2006

shells and is generally close to 400 °C.[11,12] The physicochemical characteristics of fluorinated MWCNT and their potential application as cathode material in primary lithium batteries have also been described.[13,14]

In comparison to the fluorination of MWCNTs, the structure of SWCNTs favors fluorination for temperatures as low as 50 °C.[15,16] Nevertheless, this structure is partially destroyed above 350 °C.

Fluorinated carbons are commercially used as a positive electrode material in primary lithium batteries.[2,3,17] Because highly fluorinated carbons are insulators, carbon black is added to the electrode composite in order to ensure electronic conduction. The nature and content of carbon black must be optimized to enhance the electrochemical performance of the composite electrode. Another method consists of limiting fluorination to the surface of nanomaterials such as MWCNT or carbon nanofibers (CNF). In this case, the non-fluorinated core ensures electronic conductivity, whereas the external parts are electrochemically active during discharge, following

$$(C_xF)_n + n\mathrm{Li}^+ + n\mathrm{e}^- \rightarrow n\mathrm{LiF} + nx\mathrm{C}$$

For these partially fluorinated nanomaterials, the combination of these two phenomena allows high energy and high power densities to be obtained. For large capacities, the fluorination temperature must be optimized to obtain a high fluorine content (i.e., F:C molar ratio). However, the penetration of F beneath the surface should be limited.

In this work, we have studied the reactivity of CNFs with pure fluorine gas in the 380−480 °C temperature range. The fluorinated compounds were characterized by different techniques, including (1) XRD, TEM, and Raman spectroscopy; (2) $^{19}$F and $^{13}$C high-resolution nuclear magnetic resonance ; and (3) electron paramagnetic resonance. The cross data analysis gives new insights on the mechanism of fluorination, crystal structure, and the nature of the C−F bonding. The properties of the resulting materials will be discussed and compared to those of conventional $(CF)_n$ and $(C_2F)_n$ graphite fluorides, also prepared for this study.

## 2. Experimental Section

High purity (>90%) carbon nanofibers, 2−20 $\mu$m in length, were supplied courtesy of the MER Corporation, Tucson, AZ. They were obtained by chemical vapor deposition (CVD) and heat treated at 1800 °C in an argon atmosphere to enhance their crystallinity. Fluorinated carbon nanofibers (denoted CNF−$FT_F$) were prepared with 200 mg of CNFs at temperatures ($T_F$) ranging between 380 and 480 °C in a $F_2$ stream. A reaction time of 16 h was used. The fluorination level $x$ (i.e., F:C molar ratio) was determined by gravimetry (weight uptake) and by quantitative $^{19}$F NMR measurements.

X-ray diffraction (XRD) powder patterns were obtained using a Siemens D501 diffractometer with Cu($K_\alpha$) radiation ($\lambda = 1.5406$ Å).

NMR experiments were performed with Tecmag Discovery and Bruker Avance spectrometers, with working frequencies for $^1$H, $^{13}$C, and $^{19}$F of 300.1, 73.4, and 282.2 MHz, respectively. Two NMR Bruker probes were used: a static and a special cross polarization/magic angle spinning probe with fluorine decoupling on a 4 mm rotor. The $^{19}$F−$^{13}$C match was optimized on polytetrafluoroethylene (PTFE); the $^{19}$F $\pi/2$ pulse width was 4 $\mu$s. For MAS spectra, a simple sequence ($\tau$-acquisition) was used with a single $\pi/2$ pulse length of 3.5, 4, and 3.5 $\mu$s for $^1$H, $^{19}$F, and $^{13}$C, respectively. $^{19}$F spin−lattice relaxation time $T_1$ was measured using a saturation recovery sequence and calculated taking into account a magnetization curve evolving as $\exp(-t/T_1)$. $^1$H and $^{13}$C chemical shifts were externally referenced to tetramethylsilane (TMS). $^{19}$F chemical shifts were referenced with respect to $CFCl_3$. To confirm the molar ratio F:C obtained by weight uptake and determine the limit of this method, in particular for the highest fluorination temperature for which partial exfoliation and departure of volatile fluorides can occur, we carried out quantitative $^{19}$F NMR measurements using the same conditions for each sample, i.e., similar receiver gain, recycling time $D_1$ ($D_1 > 5T_1$ using the longest spin−lattice relaxation time $T_1$, which corresponds to CNF-F480, so $D_1 = 3$ s) and scan number. The intensities are divided by the sample mass. For comparison, two conventional $(CF)_n$ samples, obtained by direct reaction of natural graphite and petroleum coke with fluorine gas at 600 °C, and a $(C_2F)_n$ sample, obtained by direct reaction of natural graphite with fluorine gas at 380 °C, with compositions $CF_{1.1}$, $CF_{1.0}$, and $CF_{0.6}$, respectively were also analyzed by quantitative NMR. Polyvinyldifluoride $(CF_2-CH_2)_n$ was used as a reference for the fluorine content.

EPR spectra were performed with a Bruker EMX digital X band ($\nu = 9.653$ GHz) spectrometer. Diphenylpicrylhydrazil (DPPH) was used as the calibration reference to determine both the resonance frequency and the densities of spin carriers.

Raman spectra were recorded at room temperature using a JOBIN YVON T64000 with a charge-coupled device multichannel detector. The radiation source was a 514.5 nm argon laser line. The laser power was tuned to 10 mW.

The different samples were characterized by transmission electron microscopy (TEM, FEI CM200 operating at 200 kV). The carbon nanofibers were dispersed in chloroform using an ultrasonic treatment, and a few drops of suspension were deposited onto copper observation grids covered with ultrathin carbon/Formvar films. The grids were subsequently dried at ambient conditions.

The quantitative analysis of TEM images was performed in reciprocal space. The details of the method can be found elsewhere.[18] The two-dimensional power spectral density function PSD ($P_2(s)$) was computed from TEM images (u($r$)) up to the critical, or Nyquist, frequency, depending on the experimental sampling interval as

$$P_2(s) \equiv \frac{1}{A}\left|\int_A u(r)W(r)\exp(2\pi isr)d^2r\right|^2 \qquad (1)$$

where $A$ denotes the image area, W($r$) window function,[19] and $s$

(11) Hamwi, A.; Alvergnat, H.; Bonnamy, S.; Béguin, F. *Carbon* **1997,** *35*, 723.
(12) Nakajima, T.; Kasamatsu, S.; Matsuno, Y. *Eur. J. Solid. State Inorg. Chem.* **1996**, *33*, 831.
(13) Hamwi, A.; Gendraud, P.; Gaucher, H.; Bonnamy, S.; Béguin, F. *Mol. Cryst. Liq. Cryst.* **1998**, *310*, 185.
(14) Touhara, H.; Inahara, J.; Mizuno, T.; Yokoyama, Y.; Okanao, S.; Yanagiuch, K.; Mukopadhyay, I.; Kawasaki, S.; Okino, F.; Shirai, H.; Xu, W. H.; Kyotani, T.; Tonita, A. *J. Fluorine Chem.* **2002**, *114*, 181.
(15) Mickelson, E. T.; Huffman, C. B.; Rinzler, A. G.; Smalley, R. E.; Hauge, R. H.; Margrave, J. L. *Chem. Phys. Lett.* **1998**, *296*, 188.
(16) Kelly, K. F.; Chiang, I. W.; Mickelson, E. T.; Hauge, R.; Margrave, J. L.; Wang, X.; Scueria, G. E.; Radloff, C.; Halas, N. J. *Chem. Phys. Lett.* **1999**, *313*, 445.
(17) Hamwi, A.; Guérin, K.; Dubois, M. *Fluorinated Materials for Energy Conversion*; Elsevier: Oxford, U.K., 2005.
(18) Basire, C.; Ivanov, D. A. *Phys. Rev. Lett.* **2000**, *85*, 5587.
(19) Press, W. H.; *Numerical Recipes in C, The Art of Scientific Computing*; Plenum Press: New York, 1988.

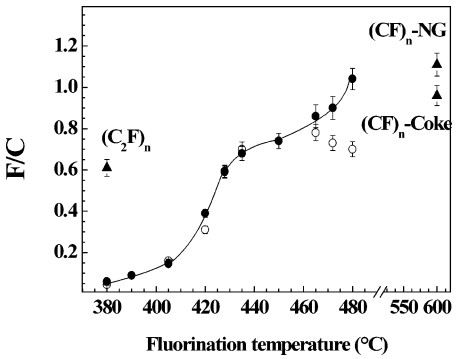


**Figure 1.** Evolution of the F:C molar ratio estimated by both weight uptake (o) and quantitative NMR data (●). The line was added to guide the eye, and triangles refer to conventional graphite fluorides $(C_2F)_n$ and $(CF)_n$ ($(CF)_n$−NG and $(CF)_n$−Coke obtained starting from natural graphite and petroleum coke, respectively).

**Table 1. F:C Ratio Obtained by Weight Uptake and Quantitative NMR Together with Raman Ratio $I_D$:$I_G$ of the Various Fluorinated CNFs**

| | | F:C | | |
|---|---|---|---|---|
| | $T_F$ (°C) | gravimetry | NMR | $I_D/I_G$ |
| CNF-F380 | 380 | 0.04 | 0.06 | 0.30 |
| CNF-F390 | 390 | 0.09 | 0.09 | 0.29 |
| CNF-F405 | 405 | 0.16 | 0.15 | 0.26 |
| CNF-F420 | 420 | 0.31 | 0.39 | 0.78 |
| CNF-F428 | 428 | 0.59 | 0.59 | 0.89 |
| CNF-F435 | 435 | 0.70 | 0.68 | 1.02 |
| CNF-F450 | 450 | 0.74 | 0.74 | 1.12 |
| CNF-F465 | 465 | 0.78 | 0.86 | 0.90 |
| CNF-F472 | 472 | 0.73 | 0.90 | fluorescence |
| CNF-F480 | 480 | 0.70 | 1.04 | fluorescence |
| CNF-F490 | 490 | partial decomposition | | |

the 2D reciprocal space vector. The $P_2(s)$ function was then transformed into the one-dimensional PSD ($P_1(s)$), where $s$ stands for the norm of $s$, according to

$$P_1(s) = (2\pi s)^{-1} \int P_2(s')\delta(|s'| - s)ds' \qquad (2)$$

## 3. Results

**3.1. Fluorination Process.** *3.1.a. Chemical composition vs Fluorination Temperature ($T_F$).* The F:C ratios of the sample, obtained from weight uptake and NMR data, are plotted as a function of the fluorination temperature in Figure 1; the values are also summarized in Table 1. The two methods yield similar results for $T_F$ up to 450 °C. At higher temperatures, however, a large discrepancy between the two methods appears, as gravimetry underestimates the actual amount of fluorine, which is more accurately determined by NMR. In fact, the NMR method was tested with two standard graphite fluorides based on $(CF)_n$ and $(C_2F)_n$ compounds and gives the correct F:C ratio. The origin of discrepancy most likely comes from the thermal decomposition of fluorinated CNFs at $T > 450$ °C, which generates volatile alkyl fluorides such as $CF_4$, $C_2F_6$, and others and, consequently, results in weight loss. In conclusion, by quantitative NMR data, the drastic increase in the fluorine content for $T_F$ higher than 420 °C is clearly demonstrated. However, a progressive increase of the fluorine content with treatment temperature is then registered contrary to what is found by weight uptake.

Four fluorination temperature zones can be distinguished in Figure 1 and Table 1: (i) for $T_F$ lower than 420 °C, the fluorination level is low ($0 < x < 0.2$); in particular, for $T_F = 380$ °C, the composition is $CF_{0.04}$, whereas for graphite at the same reaction temperature, $CF_{0.60}$ is achieved.[20] (ii) When $T_F$ is in the 420−435 °C range, the F:C ratio is drastically increased to $0.31 < x < 0.7$. (iii) When $T_F$ is included between 435 and 450 °C, the F:C ratio is nearly constant at $x \approx 0.7-0.8$. (iv) For $T_F$ higher than 450 °C, a jump in composition is observed up to 465 °C, and the latter reaches a value at $x \approx 1.0$. Finally, at 490 °C, a partial exfoliation occurs, resulting in a partial decomposition of the fluorinated carbon nanofibers.

Contrary to SWCNTs, MWCNTs and larger diameter CNTs react with fluorine at higher temperatures because of their graphitic structure. Indeed, SWCNTs react with fluorine at a temperature as low as 50 °C to form the $CF_{0.114}$ compound.[15,16] For MWCNTs, the greater the number of shells, the higher the reaction temperature with fluorine.[11] In our case, the number of graphene layers (similar to shells in MWCNT) of the pristine CNFs is about 35. This value demonstrates a high graphitization degree for the CNFs.

A surface fluorination of CNFs probably occurs during the first temperature range, whereas fluorination of the less-accessible graphene layers takes place during the second temperature range. In order to confirm this interpretation, different physicochemical characterizations were investigated at increasing $T_F$ values.

*3.1.b. Layer Stacking Structure and Morphology.* TEM bright-field images of the posttreated CNFs underline the structural order by showing the presence of graphitic layers (Figure 2a). The well-defined periodicity of the layers is reflected by a Bragg peak in the corresponding PSD curve (Figure 3), which is positioned at about 0.34 nm. The diameter distribution is quite narrow, included between 80 and 350 nm (Figure 2b). The average diameter ($<\Phi>$) is estimated to be near 150 nm from observations of various parts of the raw sample. Because of the accommodation of the fluorine atoms within the graphene layers, fluorination results in a moderate increase in the average diameter after reaction at 420 °C ($<\Phi> = 160$ nm), and to a larger extent at 480 °C ($<\Phi> = 180$ nm). The graphitic structure is maintained for fluorination at 420 °C (Figure 2c), contrary to fluorination at 480 °C (Figure 2d). For CNF-F420, the fiber morphology shows two different structures present at the periphery and in the core of the fiber. The PSD function (Figure 3), corresponding to the image in Figure 2c, displays a broad peak with a maximum at about 1.5−2.0 $nm^{-1}$ (trace 2) in addition to the usual graphene layer periodicity found for the untreated sample (Figure 2a and trace 1 on Figure 3). This additional feature in the PSD curve indicates the presence of layers, which are less ordered and are more spatially separated because of the accommodation of fluorine atoms. Note that the fiber core of the same sample does not exhibit this increased periodicity (Figure 3, trace 3).

By considering the crystalline order and the graphene layers orientation resulting from the posttreatment at 1800

(20) Dubois, M.; Giraudet, J.; Guérin, K.; Hamwi, A.; Fawal, Z.; Pirotte, P.; Masin, F. *J. Phys. Chem. B* **2006**, *110*, 11800.

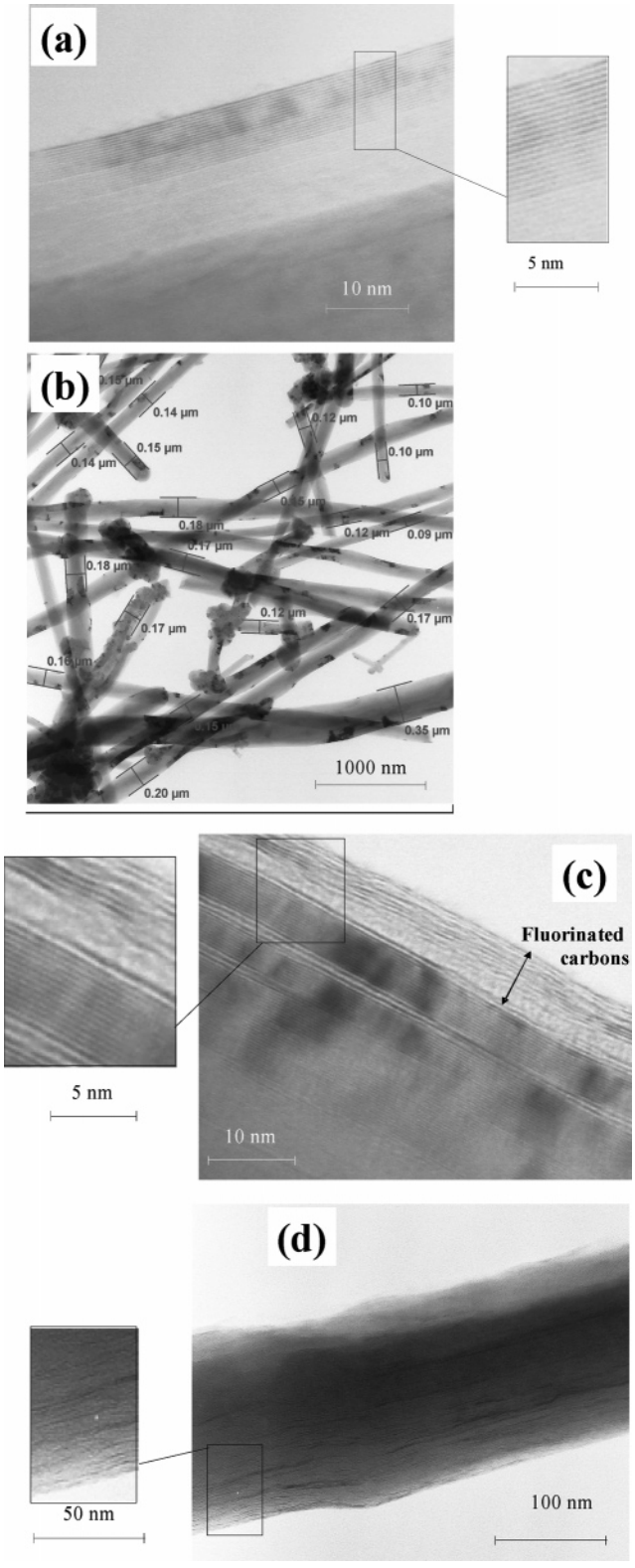


**Figure 2.** (a,b) TEM bright field images of the pristine carbon nanofibers of the fluorinated samples at (c) 420 and (d) 480 °C.

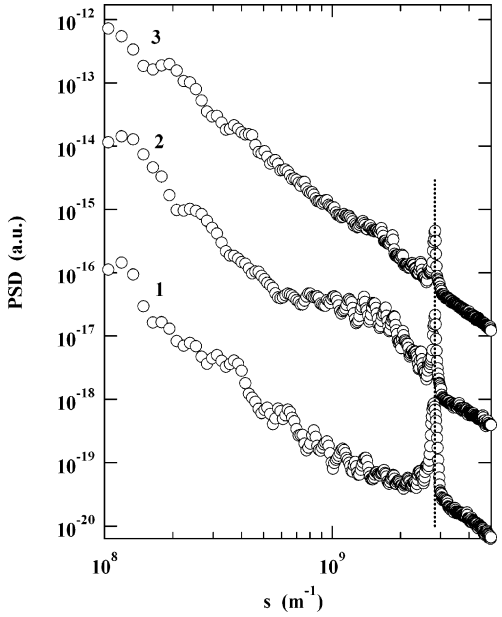


**Figure 3.** Power spectral density (PSD) functions calculated for the TEM images of Figure 2: pristine carbon nanofibers (1), fluorinated sample treated at 420 °C (2 and 3). The curves 2 and 3 correspond, respectively, to the entire image in Figure 2c and to the core of the fiber exclusively. The curves are offset vertically for clarity. The dotted line indicates the periodicity of graphitic layers.

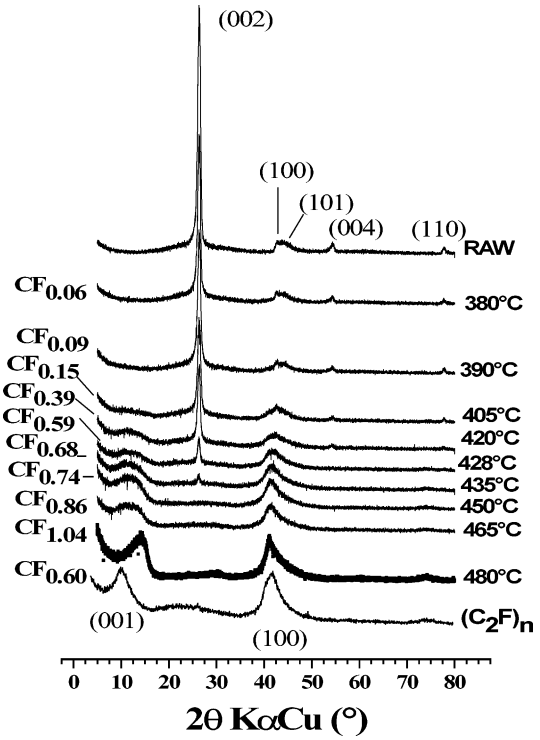


**Figure 4.** X-ray diffraction patterns of CNFs fluorinated at temperatures ranging between 380 and 480 °C compared with the $(C_2F)_n$ and $(CF)_n$ patterns.

°C, the pristine nanofibers and MWCNTs have many things in common. So, calculation similar to those applied for MWCNTs will be discussed in the following parts.

**3.2. Structural Evolution.** XRD patterns of pristine and fluorinated CNFs are compared in Figure 4. The pristine CNFs pattern is similar to that of MWCNTs synthesized by the arc discharge[21] or by CVD.[12] The main peaks correspond to the graphite (002), (100), (101), (004), and (110) diffraction lines for $2\theta$ values of 26° (interlayer distance $d = 0.338$ nm), 43° (0.207 nm), 45° (0.201 nm), 54° (0.169 nm), and 77° (0.123 nm), respectively. The strongest (002) reflection

(21) Okotrub, A. V.; Yudanov, N. F.; Chuvilin, A. L.; Asanov, I. P.; Shubin, Y. V.; Bulusheva, L. G.; Gusel'nikov, A. V.; Fyodorov, I. S. *Chem. Phys. Lett.* **2000**, *323*, 231.

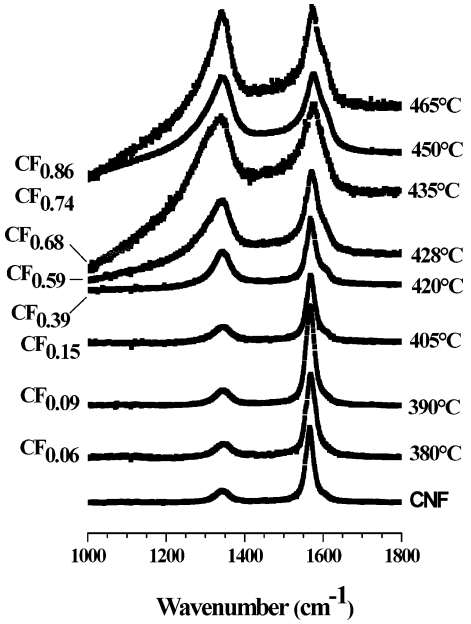


**Figure 5.** Raman spectra of CNFs fluorinated at temperatures ranging between 380 and 465 °C compared with CNFs patterns.

is associated with an average interlayer spacing of 0.338 nm, in agreement with the TEM bright-field results. The width of the (002) peak ($\Delta 2\theta = 0.72°$) characterizes both the average number of carbon layers (close to 35) and the coherence length $L_c$ along the *c*-axis (11.8 nm). As for MWCNTs, the symmetry of the (*hk*0) lines and the weak intensity of the (*hkl*) peaks reflect the lack of positional correlation between carbon atoms in different layers of a nanoparticle. The fluorination of CNFs progressively changes the structure as a function of $T_F$, as shown by the XRD. For $405 < T_F < 420$ °C, a new phase appears with corresponding peaks at $2\theta$ values centered at 12.0° and 41.5° attributed to the (001) and (100) peaks of a fluorographite matrix in a hexagonal system. This phase coexists with that of the pristine CNFs. However, the observed peak broadening of this new phase may be caused by lower stacking order of the fluorinated layers. For $435 < T_F < 450$ °C, the pristine CNFs phase disappears and only the fluorinated nanofiber phase is present. The fluorinated CNFs exhibit an interlayers spacing of 0.72 nm, which ranges between that of $(C_2F)_n$ (*d*-spacing of 0.81 nm) and that of $(CF)_n$ (*d*-spacing equal to 0.60 nm).[7] For $T_F$ of about 480 °C, a $(CF)_n$-like structure is obtained with an interlayer spacing of 0.60 nm.

In Figure 5, the Raman spectra of the fluorinated CNFs are compared with that of the starting CNFs. The latter exhibits two bands: one at 1345 $cm^{-1}$ attributed to the D mode and a second one at 1570 $cm^{-1}$ corresponding to the G mode and assigned to a double resonance Raman effect in $sp^2$ carbon atoms. In MWCNTs, the D band probably originates primarily from defects in the tube walls.[22] However, both in the tube walls and in other forms of carbon, the contribution of defects to the D band is still not completely understood. The G mode is due to an optical in-plane lattice vibration with $E_g$ symmetry of the Raman active graphitic mode. As reported by Rao et al.,[23] no Raman active vibrational modes for either fluorine or carbon-fluorine bonds exist between 1250 and 1700 $cm^{-1}$.

As the F:C ratio increases, so does the intensity of the D band. For temperatures lower than 420 °C, the CNF−$FT_F$ spectra are similar to those of CNFs. More particularly, the $I_D$:$I_G$ ratio of the integrated intensity of the D and G bands is nearly constant ($I_D$:$I_G \approx 0.30$, Table 1) within experimental error. This ratio relates to the structural disorder in CNFs. Therefore, as fluorination proceeds, the $I_D$:$I_G$ ratio increases and so does disorder. For $420 < T_F < 435$ °C, disorder is drastically increased (see Table 1), and a new mode appears at around 1620 $cm^{-1}$. This weak intensity feature was reported using a high phonon density of states for the midzone phonons near 1620 $cm^{-1}$.[23,24] For $435 < T_F < 465$ °C, the disorder-induced D band increases, but moderately, and the ratio $I_D$:$I_G$ reaches a maximum of 1.12. Finally, for $T_F$ values higher than 465 °C, Raman spectra of the resulting materials cannot be recorded because of fluorescence phenomena.

Complementary to XRD measurements, Raman spectroscopy underlines the decrease in structural coherency caused by fluorine bonding. Further proof of this evolution is provided by the investigation of the average crystal planar domain size ($L_a$) obtained using the inverse relation between domain size and the intensity ratio $I_D$:$I_G$ given by Knight and White.[25] The $L_a$ value decreases substantially from 14.7 nm for CNFs to 3.9 nm for CNF-F480.

**3.3. Solid-State NMR.** Except in the case of CNF-F380, for which the static $^{19}F$ NMR spectrum shows two asymmetric contributions at −170 and −190 ppm/ $CFCl_3$, all spectra exhibit similar shape regardless of the fluorination temperature (Figure 6). The $^{19}F$ NMR's full width at half-maximum (fwhm), of similar value ($5 \times 10^4$ Hz) for all samples, is explained by a strong dipolar homonuclear coupling between fluorine nuclei, such as that found in other fluorinated carbons as covalent graphite fluorides: $(C_2F)_n$ and $(CF)_n$,[20,26−31] semi-ionic compounds,[30,31] and fluorinated charcoal.[27,32] The center of this symmetrical resonance peak is located at −190 ppm and attributed to fluorine atoms covalently bonded to carbon atoms.[20,30,31] The increase in the fluorine nuclei content occurs without a significant change in peak shape, indicating a similar environment for fluorine atoms even though the F:C ratios are different. The case of CNF-F380 is different because two groups of fluorine nuclei are detected ($\delta = -170$ and −190; insert in Figure

(22) Osswald, S.; Flahaut, E.; Ye, H.; Gogotsi, Y. *Chem. Phys. Lett.* **2005**, *402*, 422.
(23) Rao, A. M.; Fung, A. W. P.; di Vittorio, S. L.; Dresselhaus, M. S.; Dresselhaus, G.; Endo, M.; Oshida, K.; Nakajima, T. *Phys. Rev. B* **1992**, *45*, 6883.
(24) Chieu, T. C.; Dresselhaus, M. S.; Endo, M. *Phys. Rev. B* **1982,** *26*, 5867.
(25) Knight, D. D.; White, W. S. *J. Mater. Res.* **1989**, *4*, 385.
(26) Panich, A. M. *Synth. Met.* **1999**, *100*, 169.
(27) Touhara, H.; Okino, F. *Carbon* **2000**, *38*, 241.
(28) Panich, A. M.; Shames, A. I.; Nakajima, T. *J. Phys. Chem. Solids* **2001**, *62*, 959.
(29) Krawietz, T. R.; Haw, J. F. *Chem. Commun.* **1998**, *19*, 2151.
(30) Dubois, M.; Guérin, K.; Pinheiro, J. P.; Fawal, Z.; Masin, F.; Hamwi, A. *Carbon* **2004**, *42*, 1931.
(31) Giraudet, J.; Dubois, M.; Guérin, K.; Pinheiro, J. P.; Hamwi, A.; Stone, W. E. E.; Pirotte, P.; Masin, F. *J. Solid State Chem.* **2005**, *118*, 1262.
(32) Hagaman, E. W.; Murray, D. K.; Cul, G. D. D. *Energy Fuel* **1998**, *12*, 399.

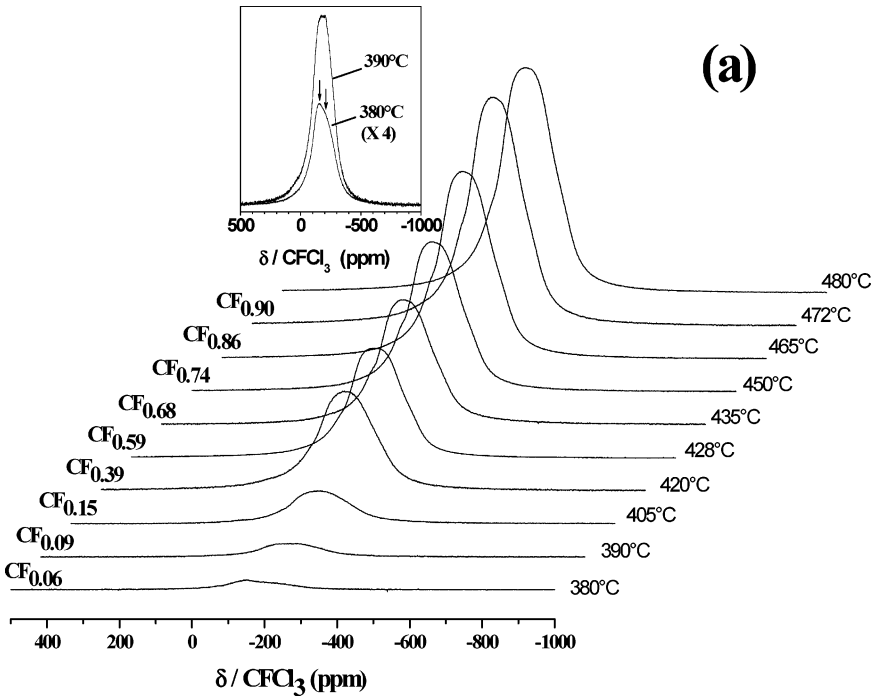


**Figure 6.** Static $^{19}F$ NMR spectra of CNF−$FT_F$ (380 < $T_F$ < 480 °C). The insert in (a) shows the spectra of the lowest fluorinated samples ($T_F$ = 380 and 390 °C).

6); they result from either different interactions between carbon and fluorine atoms or different environments. The intercalation of mobile $F^-$ resulting from traces of HF molecules cannot be excluded as in the case of $(C_4F)_n$ type.[26] The low fluorine content (F:C = 0.04) may lead then to inhomogeneous fluorination at the CNF surfaces.

The room-temperature $^{19}F$ MAS NMR spectra of CNF−$FT_F$ recorded at a spinning rate of 10.0 kHz are displayed in Figure 7. The spectrum for $(C_2F)_n$ is also added to show its strong similarity with fluorinated CNFs. CNF-F428's fwhm (6800 Hz) is larger than that of any of the other fluorinated samples (4100 Hz). This can be explained by the efficiency of the MAS experiment, which depends on the structural order of the studied sample; this particular compound is less ordered, as revealed by XRD. $(C_2F)_n$ and all types of CNFs studied above 428 °C exhibit similar MAS spectra and are hence unaffected by the degree of fluorination. This confirms that both C−F bonding and the fluorine environment are similar in these samples. An intense isotropic peak at −190 ppm/$CFCl_3$ is present, together with its spinning sidebands. This peak corresponds to fluorine atoms involved in covalent C−F bonds. This covalent character was confirmed by FT−IR spectroscopy (not shown here), which shows a vibration band at 1215 $cm^{-1}$, assigned to the covalent C−F bond in $(C_2F)_n$.[8]

A second, less-intense resonance at −120 ppm (present as a shoulder on one of the spinning sidebands of the C−F line) indicates the presence of $CF_2$ groups. Nevertheless, the content of the $CF_2$ groups is small but sufficient to be detected by $^{19}F$ MAS NMR. The sidebands of the $>CF_2$ resonance are also present, in particular the one superimposed on the left side of the isotropic peak of the C−F groups and resulting in a shoulder. These groups could be assigned to either fluorine atoms located at the edge of graphite layers or structural defects. These $^{19}F$ MAS experiments allow other

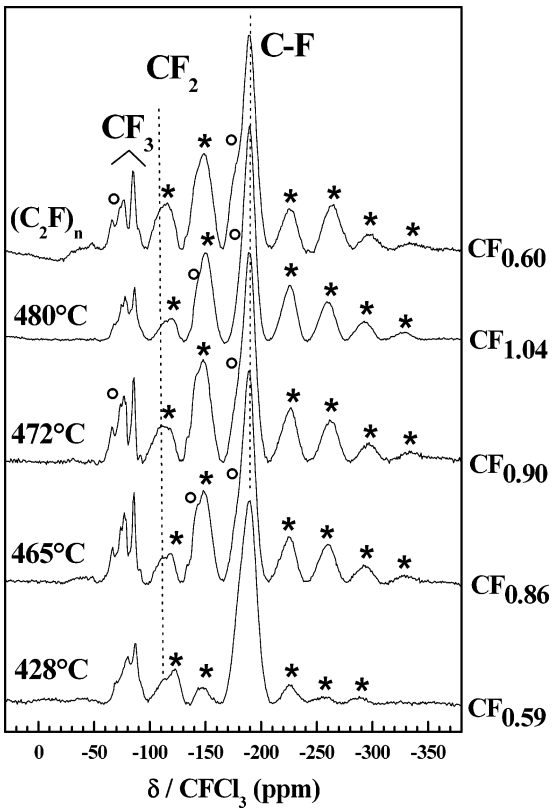


**Figure 7.** $^{19}F$ MAS NMR spectra of CNF−$FT_F$ and $(C_2F)_n$ graphite fluoride with 10 kHz spinning rate; the * and ○ markers denote spinning sidebands related to the isotropic peaks at −190 and −120 ppm, respectively.

groups ($CF_3$) to be detected in spite of their very low levels present. Several narrow lines are present in the −60 to −90 ppm range, superimposed with spinning sidebands of C−F and $>CF_2$ peaks. These groups can be localized on the fluorocarbon sheet edges and probably possess a spinning motion around the C−C bonds, explaining the narrowness of the resonance.

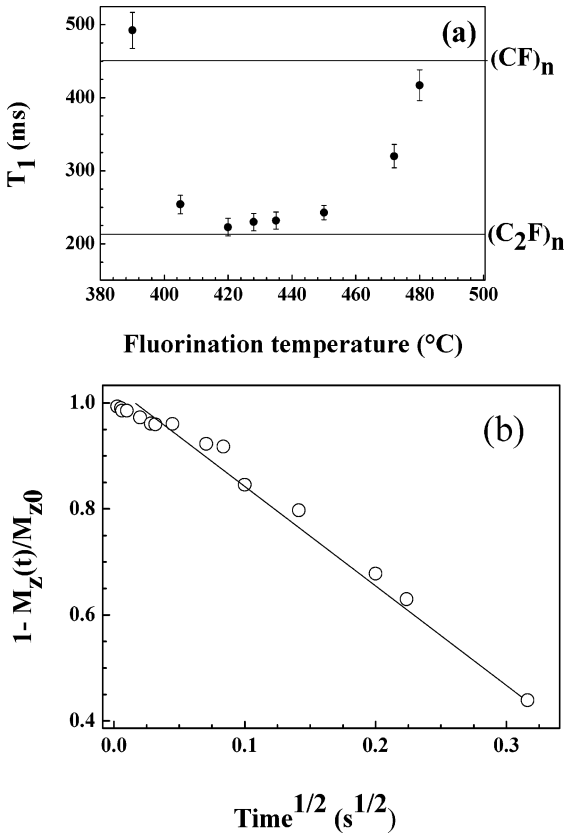


**Figure 8.** Evolution of (a) the spin−lattice relaxation time $T_1$ as a function of the fluorination temperature and of (b) the initial $^{19}$F magnetization curve of CNF-F420, $1 - M_z(t)/M_{z0}$ vs $t^{1/2}$.

The evolution of the$^{19}$ F spin−lattice relaxation time ($T_1$) with fluorination temperature shown in Figure 8a gives complementary information about the fluorine accommodation if the values are compared to those of conventional high-temperature graphite fluoride types $(CF)_n$ and $(C_2F)_n$, which are equal to 450 and 210 ms, respectively.[20,33] For a large range of fluorination temperatures ($405 < T_F < 450$ °C), i.e., those corresponding to a large range of F:C ratios from 0.16 to 0.74, the spin−lattice relaxation times are close to the value found in $(C_2F)_n$ (Figure 8a). This fact, in accordance with the other characterizations, suggests a fluorination mechanism involving $(C_2F)_n$ formation and its propagation toward the core without major structural change. This assumption will be confirmed below by $^{13}$C MAS NMR experiments. Hence, when the reaction temperature is increased to 480 °C, $T_1$ progressively approaches a 450 ms value, which is similar to that measured in $(CF)_n$ prepared using petroleum coke. The conversion from $(C_2F)_n$ type to $(CF)_n$ type structure goes through a partial exfoliation of fluorinated layers to allow for additional fluorine uptake.

The case of CNF-F390 is special because the fluorine content is very low (F:C = 0.09) and the fluorinated parts are located essentially on the CNFs surface. We believe that the external surface is heavily fluorinated and could explain the high $T_1$ value (492 ms) registered for this compound.

Contrary to $(CF)_n$ carbon fluoride (fluorinated coke), the presence of paramagnetic centers is an important factor of relaxation in the case of $(C_2F)_n$.[20,28,33] Such a process is underlined by the linearity of the magnetization curve $1 - M_z(t)/M_0$ vs $t^{1/2}$ for short recovery times (Figure 8b). In fact, under certain conditions when the spin diffusion constant is of appropriate value, the magnetization for short recovery times develops as $t^{1/2}$.[34] This curve is linear for all fluorinated CNFs, as exemplified by the sample obtained at 420 °C, giving additional proof of the structural similarities between CNF−$FT_F$ and $(C_2F)_n$.

$^{13}$C MAS NMR gives additional information about the nature of the interaction between carbon and fluorine atoms, i.e., the C−F bonding, and the presence of non-fluorinated carbon atoms. Here again, the lowest fluorinated sample (CNF-F380) differs from the other CNF−$FT_F$ compounds, because it exhibits only one broad resonance centered near 120 ppm/TMS (Figure 9a). Such a shape is close to that of pure graphite. Because of the low fluorine content, only a small part of the carbon atoms are bonded to fluorine atoms. When the fluorine content reaches 0.16, the line becomes asymmetric and two well-defined resonances are present at 84−88 and 42 ppm for F:C ≥ 0.31, both related to carbon atoms exhibiting $sp^3$ hybridization. The first line (with area denoted $S_{CF}$) is assigned to carbons atoms covalently bonded to fluorine atom, as expected from the fluorine content found in this range of temperatures.[26,30,31] The other peak is related to non-fluorinated $sp^3$ carbons atoms (C $sp^3$), as in the case of $(C_2F)_n$.[20] A chemical shift of 42 ppm corresponds to $sp^3$ carbon atoms as proposed by Wilkie et al.[35] for $(C_xF)_n$ ($x > 1$). In accordance with the proposed structural model of $(C_2F)_n$, which consists of fluorographite layers connected in pairs by interlayer covalent C−C bonds,[36,37] this line could be attributed to $sp^3$ carbon atoms. As only half of the carbon atoms are fluorinated, $sp^3$ hybridized carbon atoms are exclusively bonded to other carbons. The resonance peak of pure diamond is expected at 35 ppm;[38] therefore, a weak fluorine−carbon interaction can lead to a chemical shift value similar to that observed in the case of $(C_2F)_n$ ($\delta = 42$).[1,30]

The third large resonance peak centered near 120 ppm is mainly assigned to non-fluorinated $sp^2$ carbon atoms but also to carbon atoms in low interaction with fluorine ($\delta = 140$).[1,30] So, when the fluorination temperature is lower than 480 °C, the $^{13}$C NMR spectra exhibit two contributions: (i) the resonance of the non-fluorinated core centered around 120 ppm and (ii) the lines of fluorinated parts, which are typical of $(C_2F)_n$ graphite fluoride. The ratio of these two contributions depends on the fluorination temperature and decreases with $T_F$. Similar behavior is observed for $(C_2F)_n$, because a broad line appears on the spectra that also depends on $T_F$ and is a result of the presence of residual graphite.[20]

The difference between the spectra of $(C_2F)_n$ and fluorinated CNFs, for example, with CNF-F428, comes from the non-fluorinated parts (the core for CNF and residual graphite for $(C_2F)_n$).

(33) Giraudet, J.; Dubois, M.; Guérin, K.; Hamwi, A.; Masin, F. *J. Phys. Chem. Solids* **2006**, *67* (5−6), 1100.
(34) Blumberg, W. E. *Phys. Rev.* **1960**, *119*, 79.
(35) Wilkie, C. A.; Yu, G.; Haworth, D. T. *J. Solid Sate Chem.* **1979**, *30*, 197.
(36) Watanabe, N. *Physica B* **1981**, *105*, 17.
(37) Sato, Y.; Itoh, K.; Hagiwara, R.; Fukunaga, T.; Ito, Y. *Carbon* **2004**, *42*, 3243.
(38) Duijvestjn, M. J.; Van der Lugt, C.; Smidt, J.; Wind, R. A.; Zilm, K. W.; Staplin, D. C. *Chem. Phys. Lett.* **1983**, *102*, 25.

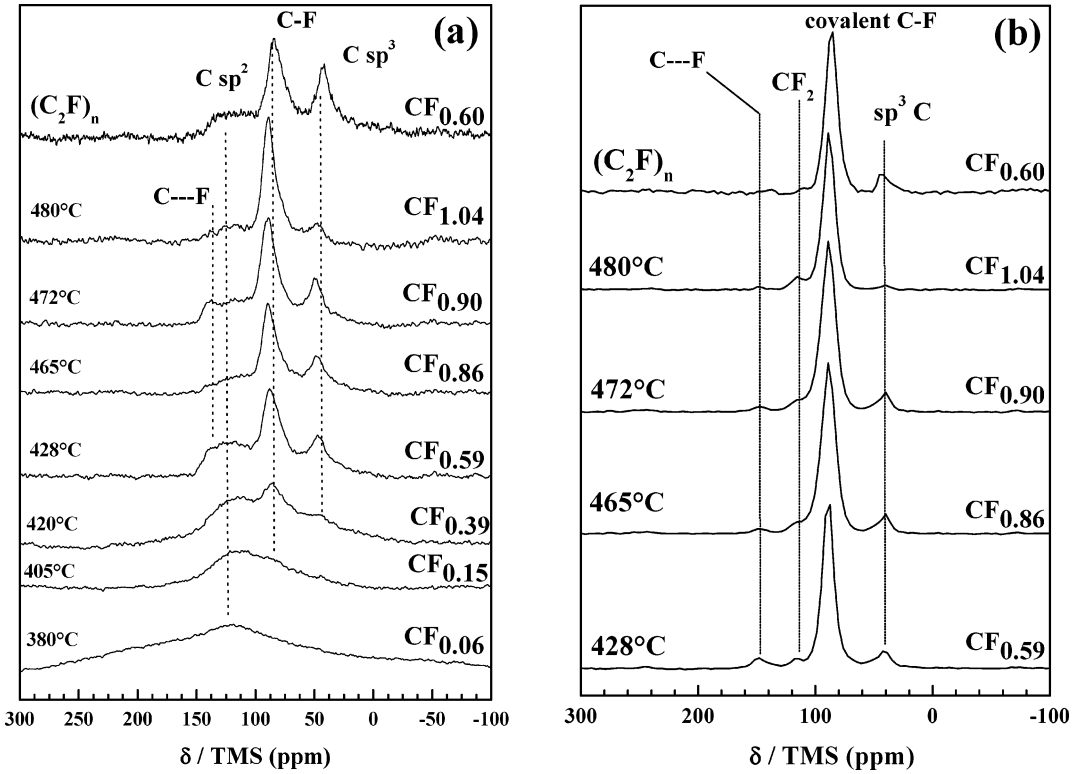


**Figure 9.** (a) $^{13}C$ MAS NMR spectra of CNFs fluorinated at temperatures ranging between 380 and 480 °C compared with the $(C_2F)_n$ graphite fluoride spectrum. (b) $^{13}C$ MAS NMR spectra of CNF−$T_F$ and $(C_2F)_n$ graphite fluoride obtained with $^{19}F$ to $^{13}C$ cross polarization (the spinning rate is 10 kHz).

It must be noted that the strong line at 42 ppm was observed only for $(C_2F)_n$ type graphite fluoride. This resonance and its intensity is solid proof of the formation of a $(C_2F)_n$ type structure in the fluorinated parts in a wide range of fluorination temperatures.

The area ratio of the two $sp^3$ carbon resonances is nearly constant regardless of the fluorine content; we have $S_{C-F}$: $S_{Csp^3} = 2.43$, 2.37, and 2.34 for CNFs fluorinated at 428, 465, and 472 °C, respectively. For comparison, the spectrum of $(C_2F)_n$ graphite fluoride is also shown (this sample was obtained by fluorination of graphite at 380 °C, exhibits a F:C ratio of 0.60, and a few $sp^2$ C have been identified).[20] In this case, the $S_{C-F}$:$S_{Csp^3}$ ratio is close to 1.5.

On the other hand, the content of $sp^2$ carbon atoms decreases continuously when the fluorination temperature increases, i.e., F:C content increases. It should be noted that such a process also occurs with $(C_2F)_n$ when the temperature is increased from 350 to 380 °C ($CF_{0.51}$ and $CF_{0.60}$, respectively).[12] Fluorination of CNFs then results in an increase in the F:C ratio without significant structural modification. The formed C−F bonds are mainly covalent.

NMR measurements performed using MAS and $^{19}F \rightarrow {}^{13}C$ cross-polarization may differentiate between the various carbon atoms. A comparison of the spectra acquired with MAS and CP-MAS for CNF−$FT_F$ and $(C_2F)_n$ (panels a and b of Figure 9) confirms our assignments for the three kinds of carbon atoms. As C−F groups are favored with CP-MAS in comparison to carbon second neighbors, i.e., $sp^3$ carbon atoms, only the peak corresponding to C−F bonds from the fluorocarbon matrix increases, contrary to both $sp^3$ hybridized carbon atoms exclusively bonded to other carbon atoms ($S_{C-C}$) and $sp^2$ graphitic carbon atoms ($S_G$), the latter completely disappearing. Considering the peak at 145 ppm, which is revealed using these conditions, the measurements also show the presence of $sp^2$ carbon atoms in weak interaction with fluorine, as in the case of room-temperature graphite fluorides.[30,31] However, these atoms are only present in very low concentrations.

Moreover, resonance of $>CF_2$ groups is also favored with CP-MAS, and a small line is observed at 110 ppm as a shoulder of the $S_{C-F}$ peak (Figure 9b). Such groups have already been observed elsewhere in various $(CF)_n$.[8,27−29,35]

Whereas the MAS spectra are similar for samples treated between 428 and 472 °C, the intensity of the peak related to $sp^3$ carbon atoms significantly decreases for CNF-F480 showing that the nature of this sample has been changed. The spectrum of CNF-F480 is very near to that observed for $(CF)_n$, contrary to the other spectra, which exhibit similarities with the $(C_2F)_n$ spectrum. This underlines the conversion of $(C_2F)_n$ into $(CF)_n$ at the higher temperatures. Nevertheless, this conversion is not achieved, resulting in the persistence of the peak of non-fluorinated carbons at 45 ppm, which is typical of $(C_2F)_n$.

The C−F bond length can be determined by NMR because these data are included in the expression of the dipolar coupling. This latter information is lost when Hartmann−Hahn cross-polarization (CP) associated with MAS is used, but the dipolar coupling can be reintroduced into the spectrum thanks to the inverse cross-polarization (ICP) sequence. This method and the experimental conditions are fully explained in a previous paper concerning $(CF)_n$.[39]

(39) Giraudet, J.; Dubois, M.; Hamwi, A.; Stone, W. E. E.; Pirotte, P.; Masin, F.; *J. Phys. Chem. B* **2005**, *109*, 175.

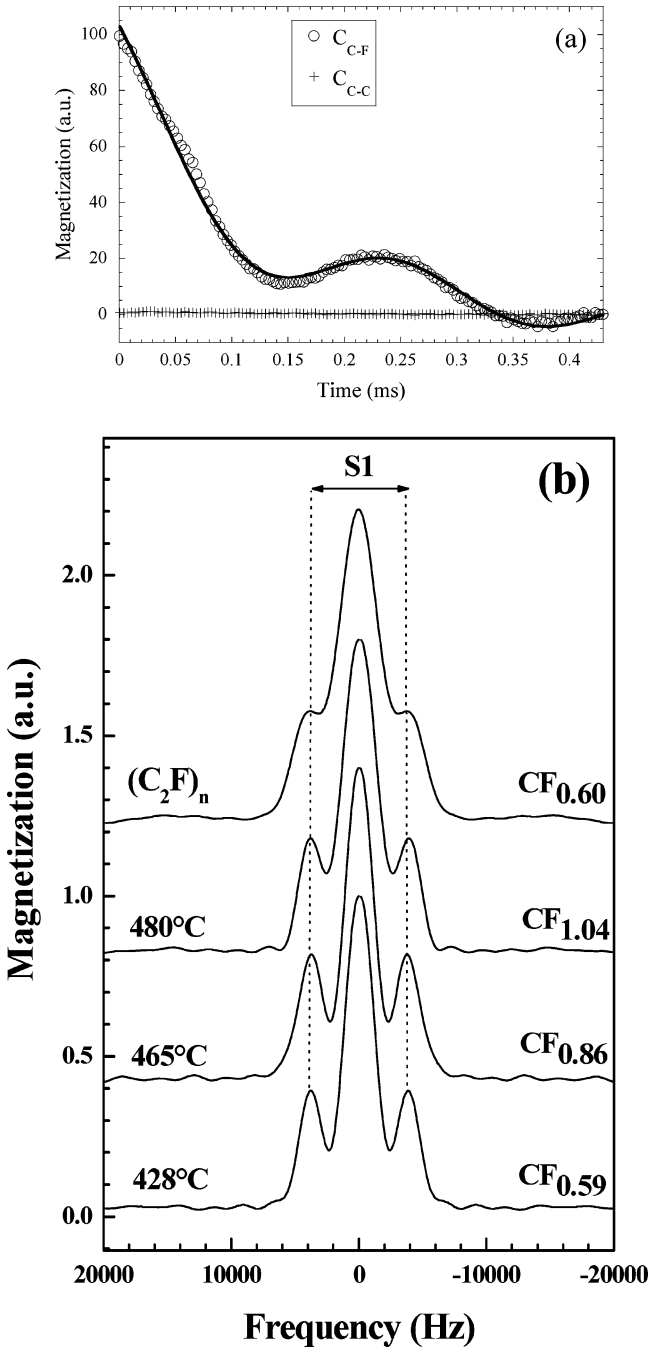


**Figure 10.** (a) Time evolution of the $^{13}C$ magnetization for carbon atoms covalently bonded to fluorine (o) and exclusively bonded to carbon ($sp^3$ C) (•) of CNF-F472 with a spinning rate of 14.5 kHz at the $n = 1$ Hartmann−Hahn condition. (b) Fourier transform of the resulting oscillation as a function of the fluorination temperature. The curve of $(C_2F)_n$ graphite fluoride is added for comparison.

For short contact times, the amplitude of the CP signal is found to be oscillatory with a frequency $\varphi$ related to the C−F bond length.[40] This behavior is observed only for carbon covalently bonded to fluorine and not for $sp^3$ carbon atoms. Using the ICP sequence, the integrated peak intensity of the carbon spectra was calculated as a function of contact time, thus revealing the CP dynamics (Figure 10a); the extracted frequency was $\varphi = 3976.0 \pm 18.6$ Hz. From $r_{CF} = \sqrt[3]{10.0463/\varphi}$[20,39,40], $r_{CF} = 0.136 \pm 0.001$ nm.

As for $(C_2F)_n$[20] and $(CF)_n$,[39] Fourier transform of the $^{13}C$ magnetization evolution for C−F groups gives the Pake-like structure for all fluorination degrees of CNFs (Figure 10b). The C−F bond length ($r_{CF}$) can be deduced from the Pake structure using the wings that are related to dipolar fluctuation. S1 is the separation between these wings. The bond length can be estimated from the equation $r_{CF} = \sqrt[3]{20.0926/S1}$ (nm).[120,39,40] The S1 value is equal to 7700 Hz for all the fluorinated CNFs samples. A C−F bond distance equal to $0.138 \pm 0.002$ nm is found in all studied cases. It must be noted that these values as estimated by NMR could be overestimated because of possible molecular motions, which decrease the value of the second moment, inversely proportional to the C−F distance. The C−F bond lengths in CNF−$FT_F$ are close to those obtained by the same NMR procedure for $(C_2F)_n$[20] and $(CF)_n$ (0.138 nm),[39] indicating that the nature of the C−F bonding is similar in these three compound types.

**3.4. EPR Study.** The pristine sample does not exhibit an EPR signal within the detection limits of the spectrometer. Figure 11a displays the EPR spectra of fluorinated CNFs. The origin of the main broad line was attributed to carbon dangling bonds having a localized spin. Such spin carriers have been proposed for other fluorinated carbons obtained in a $F_2$ atmosphere at 600 °C starting from graphite[28] or room-temperature graphite fluoride,[30,33] as well as for amorphous carbon thin film[41,42] or nanosized graphite fluorides.[43] The EPR parameters are summarized in panels a and b of Figure 12 and in Table 2. Once again, the CNFs fluorinated at the lowest and the highest temperatures ($T_F <$ 405 °C and $T_F =$ 480 °C) differ from the other samples. The spectrum of CNF-F380 is asymmetric (the A:B intensity ratio of positive and negative parts of the derivative curve is close to 0.6 (Figure 12a)). This asymmetry, revealing different contributions to the spectra, disappears gradually as fluorination is increased. So, A:B leads to 1. Simulation of the spectra reveals three contributions for CNF-F380, CNF-F472, and CNF-F480 (Figure 11b−d, respectively, and also Table 2). These simulations were performed using WinSimfonia (Bruker software).

First, by analogy with $(C_2F)_n$ and $(CF)_n$, the observed broad line 4 may be due to the combined contributions of both the dangling bonds in interaction with oxygen[20] and, in the cases of $(CF)_n$ and CNF-F480, the unresolved superhyperfine structure, which for both samples exhibits nearly the same line width.[31] Because the linewidths are close, line 2 could be related to dangling bonds located in neighboring areas, similar to those in $(C_2F)_n$ (Table 2). For the same reason, we can assign line 3 to structural defects similar to those present in $(CF)_n$.[33,39]

The spectrum of CNF-F480 exhibits three contributions: a narrow line ($\Delta H_{pp} = 17.4 \pm 0.2$ G), a broad one ($\Delta H_{pp} =$ $80 \pm 5$ G) and, contrary to the other samples, a resolved superhyperfine structure SHFS. As for $(CF)_n$, this SHFS is

(40) Bertani, P.; Raya, J.; Reinheimer, P.; Gougeon, R.; Delmotte, L.; Hirschinger, J. *Solid State Magn. Res.* **1999**, *13*, 219.
(41) Yokomichi, H.; Morigaki, K. *J. Non-Cryst. Solids* **2000**, *266*, 797.
(42) Yokomichi, H.; Hayashi, T.; Amano, T.; Masuda, A. *J. Non-Cryst. Solids* **1998**, *227*, 641.
(43) Takai, K.; Sato, H.; Enoki, T.; Yoshida, N.; Okino, F.; Touhara, H.; Endo, M. *Mol. Cryst. Liq. Cryst.* **2000**, *340*, 289.

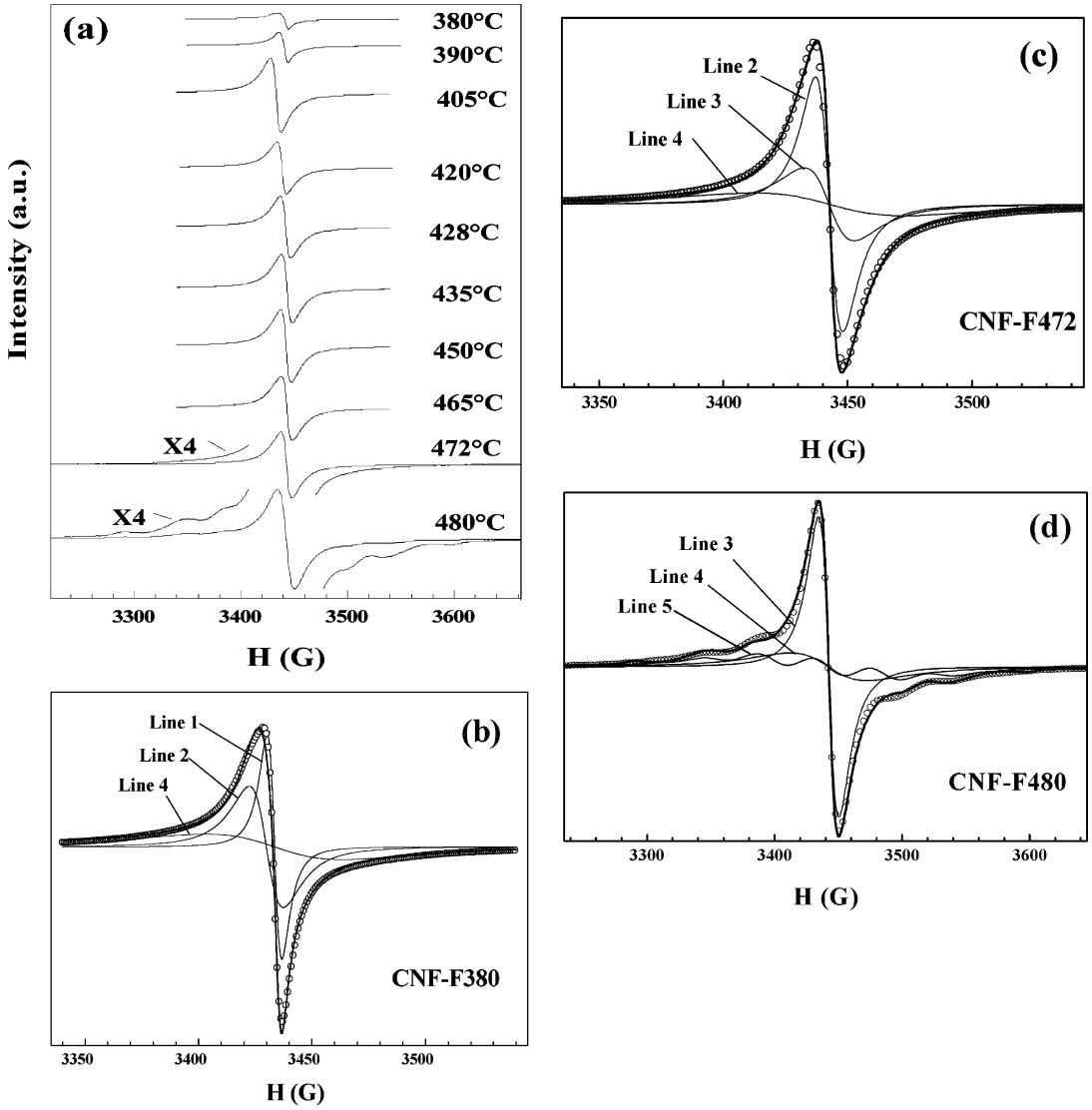


**Figure 11.** (a) EPR spectra of the fluorinated CNFs (to facilitate comparison, the intensities are divided by the sample mass) and simulations of selected samples (b) CNF-F380, (c) CNF-F472, and (d) CNF-F480.

**Table 2. Data from the EPR Spectra**

| | $\Delta H_{PP}$ (G) | | | | | | |
|---|---|---|---|---|---|---|---|
| | line 1 (± 0.2 G) | line 2 (± 0.2 G) | line 3 (± 0.2 G) | line 4 (± 5 G) | line 5 | A:B | $D_s$ (spins $g^{-1}$) |
| CNF-F380 | 6.2 | 15.0 | | 60 | | 0.6 | $0.5 \times 10^{20}$ |
| CNF-F472 | | 11.0 | 19.5 | 60 | | 1 | $2.4 \times 10^{20}$ |
| CNF-F480 | | | 17.4 | 80 | SHFS[a] | 1 | $7.7 \times 10^{20}$ |
| $(C_2F)_n$[12] | | 13.5 | | 80 | | 1 | $1.7 \times 10^{20}$ |
| $(CF)_n$[31] (from petroleum coke) | | | 20.9 | 80 | SHFS[a] | 1 | $15.6 \times 10^{20}$ |

[a] SHFS stands for superhyperfine structure with $(2nI + 1) = 7$ lines, where $n = 6$ is the number of neighboring fluorine nuclei (nuclear spin number $I = 1/2$; coupling constant $A = 45 \pm 2$ G, line width $\Delta H_{pp} = 36 \pm 2$ G[20,28,33]).

due to the hyperfine interaction between a dangling bond electron and six neighboring fluorine nuclei.[20,28,33] Such a SHFS for CNFs fluorinated at 480 °C underlines a neighboring of the dangling bonds similar to $(CF)_n$. The content of these spin carriers increases with the fluorination temperature and becomes predominant for CNF-F480 (the dangling bonds of line 2 completely disappeared). Line 1, responsible for the asymmetry (Figure 11b), appears for the lowest-temperature reaction (380 and 390 °C) when inhomogeneous fluorination occurs close to the surface. The narrowness of this signal results from different interactions with the fluorocarbon matrix and/or presence of intercalated $F^-$. On the one hand, the spin density ($D_s$, i.e., the number of dangling bonds per mass of the sample) continuously increases with the fluorination temperature, as shown in Figure 12b, because of the propagation of the fluorinated parts, which contain paramagnetic defects. It must be noted that CNFs do not exhibit EPR lines. For $T_F$ included between 380 and 472 °C, $D_s$ is close to that of $(C_2F)_n$ ($17 \times 10^{19}$ spins $g^{-1}$, see Table 2). On the other hand, $D_s$ drastically increases for CNF-F480 and becomes more and more similar to that of $(CF)_n$ type ($15.6 \times 10^{20}$ spins $g^{-1}$; this sample

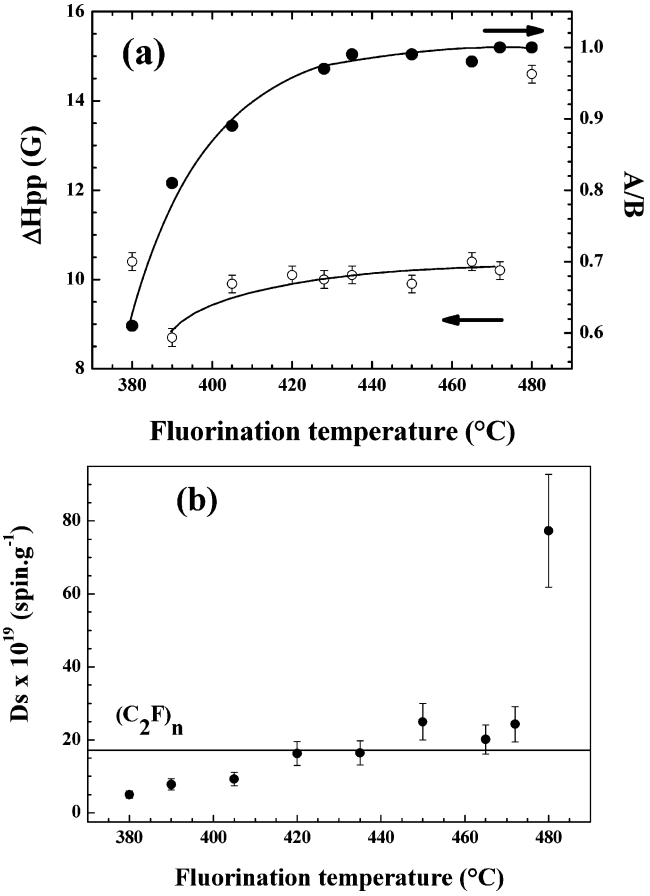


**Figure 12.** Evolution of (a) the EPR parameters (line width ($\Delta H_{PP}$) and A:B ratio) and (b) $D_s$ spin density with the fluorination temperature .

was obtained with natural graphite) in accordance with the structural conversion of $(C_2F)_n$ into $(CF)_n$, which has been proposed before in the present work.

## 5. General Discussion

The particular structure of CNFs seems to favor the formation of $(C_2F)_n$ type materials as fluorination proceeds. This $(C_2F)_n$ structure, which consists of pairs of fluorographite layers, is formed and conserved regardless of the fluorination temperature ($405 < T_F < 450$ °C), through a wide range of composition (F:C = 0.16−0.74). This feature can be explained by a fluorination process occurring close to the external walls when low temperatures are applied and then progressing toward the internal walls when the temperature is increased. This mechanism is different from that of the fluorination of graphite, as a progressive conversion from $(C_2F)_n$ into $(CF)_n$ occurs when the temperature is increased within the 350−600 °C range.[7,44] Whereas $(C_2F)_n$ and $(CF)_n$ are formed via a fluorine-intercalated phase with planar graphene layers,[44] this intermediate phase does not seem to be involved during the fluorination of CNFs. An increase in fluorination temperature up to 480 °C results in a partial decomposition of the CNFs. The mechanism could be similar to that of a partial exfoliation. The $^{13}C$ NMR spectrum (Figure 9) of this resulting material clearly shows the low contents of both the pristine $sp^2$ carbons and $sp^3$ carbon atoms related to the $(C_2F)_n$ type. The partial decomposition of the fluorinated parts leads to a conversion of $(C_2F)_n$ into $(CF)_n$, which is not totally achieved at 480 °C.

Even if the evolution of the F:C ratio for CNFs could be expected under the fluorination conditions applied here, some new and interesting features can be highlighted from this study. Contrary to previous works concerning MWCNT,[11] the high degree of purity of our raw CNFs allows the chemical composition to be accurately deduced from the F:C ratio. In the previous studies, this was underestimated because of the presence of reactive carbon in the pristine sample which formed volatile carbon−fluorine derivatives. Moreover, the F:C ratio increase within the narrow temperature range (420 − 435 °C) had never been reported before; only a high fluorination process between 400 and 500 °C had been previously suggested.[12] Furthermore, another important finding in this study is the determination of both a temperature limit before CNF decomposition and a fluorination level limit for CNFs. On the basis of complementary characterization using NMR, Raman, and XRD, we can classify the fluorinated materials into three different types, depending on the treatment temperature:

For the lowest fluorination temperatures ($T_F < 420$ °C), the fluorinated samples exhibit a low fluorine content and their structure is close to that of pristine CNFs, as shown by Raman spectroscopy and XRD. The fluorine atoms are located on the CNFs surface, i.e., on the external walls.

In the 420−465 °C temperature range, drastic changes take place as a consequence of the F:C ratio increase, which is rapid for $T < 435$ °C. The fluorination level then slows down; first, the samples become biphasic (CNF and CNF−F) and the new CNF−F phase exhibits cristallographic similarities with $(C_2F)_n$ type graphite fluoride involving paired fluorographite layers connected by interlayer covalent C−C bonds. This has been demonstrated by the presence of $sp^3$ hybridized carbon atoms exclusively bonded to carbon atoms in the fluorocarbon interlayer. The curvature of the graphene layers and/or their stacking seems to both limit the fluorination in comparison with graphite and favor the formation of this $(C_2F)_n$ type phase. Raman scattering reveals that the concentration of structural defects increases with the fluorine content. Moreover, the incorporation of fluorine atoms occurs through the formation of covalent C−F bonds. The type of interaction between carbon and fluorine atoms does not vary with the fluorine content. Therefore, the fluorination process must start from the outer walls, forming a $(C_2F)_n$ configuration, and then progresses toward the CNF core.

When the fluorination temperature is increased above 465 °C, a low exfoliation occurs and decomposes the CNF−$FT_F$, as clearly shown in the case of CNF-F480. This mechanism was evidenced by both $^{13}C$ NMR and XRD, which clearly show the conversion of $(C_2F)_n$ into $(CF)_n$ allowed by a partial exfoliation. Nevertheless, the $(C_2F)_n$ into $(CF)_n$ conversion is low for treatment temperatures equal to 472 °C and mainly occurs for $T_F \geq 480$ °C. The occurrence of fluorescence in the Raman scattering spectra may be the signature of $(CF)_n$ formation at higher $T_F$.

(44) Kupta, V.; Nakajima, T.; Ohzawa, Y.; Žemva, B. *J. Fluorine Chem.* **2003**, *120*, 143.

## 5. Conclusion

The reaction of fluorine gas with carbon nanofibers for temperatures ranging between 380 and 480 °C has been studied. Fluorine content increases from $CF_{0.31}$ up to $CF_{0.70}$ in a narrow temperature range (420−435 °C). 472 °C appears as the upper temperature before partial CNF decomposition. For lower temperatures, only a surface fluorination occurs. In order to determine which fluorinated phase is formed depending on the fluorination temperature, $^{13}C$ MAS NMR appears as a solid proof of the existence of $(C_2F)_n$ type phase in the wide range of temperatures. Moreover, when comparing $(CF)_n$ and $(C_2F)_n$ graphite fluorides, structural parameters such as interlayer distance, $^{19}F$ spin−lattice relaxation time $T_1$, paramagnetic dangling bond density, and environment are sufficiently different to enable us to determine which phase is formed during the fluorination of the carbon nanofibers as a function of temperature.

In the 420−435 °C temperature range, the samples become biphasic and the new crystallographic phase in addition to the raw CNFs exhibits some similitudes with $(C_2F)_n$ type graphite fluoride. This phase is formed regardless of the fluorine content, above a reaction temperature of 420 °C, suggesting that fluorination occurs from the external walls toward the core with increasing fluorination temperature. Moreover, the incorporation of fluorine atoms occurs through the formation of covalent C−F bonds, whatever the fluorine content.

**Acknowledgment.** The authors thank MER Corporation, Tucson, AZ, for generously providing the CNFs and Dr. William Stone from the Service de Matière Condensée et Résonance Magnétique (Université Libre de Bruxelles, Belgium) for valuable discussions concerning this work.

CM061731M